iScience

CellPress
OPEN ACCESS

Article

CRISPR interference provides increased cell type-specificity compared to the Cre-loxP system

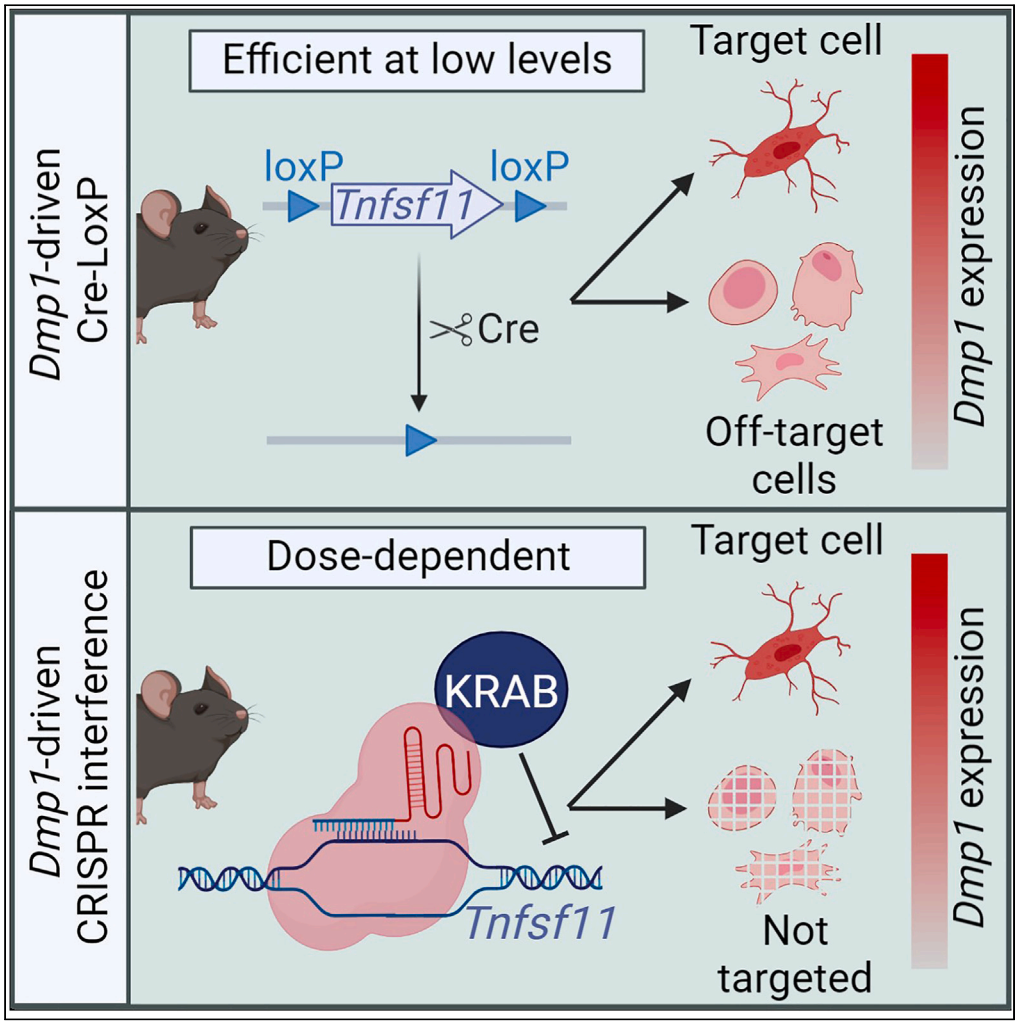

Dominique J. Laster, Nisreen S. Akel, James A. Hendrixson, ..., Intawat Nookaew, Charles A. O'Brien, Melda Onal

monal@uams.edu

Highlights

In vivo global gene knockdown by CRISPRi can be as effective as gene knockout

CRISPRi can be adapted to perform *in vivo* cell type-specific loss of function

Cell type-specific loss of function using CRISPRi is more specific than Cre-loxP

Knockdown by cell type-specific CRISPRi persists up to 12 months of age

Laster et al., iScience *26*, 107428
August 18, 2023
https://doi.org/10.1016/j.isci.2023.107428

iScience

CellPress
OPEN ACCESS

Article

CRISPR interference provides increased cell type-specificity compared to the Cre-loxP system

Dominique J. Laster,[1] Nisreen S. Akel,[1] James A. Hendrixson,[1] Alicen James,[1] Julie A. Crawford,[2,3] Qiang Fu,[2,3] Stuart B. Berryhill,[2,3] Jeff D. Thostenson,[4] Intawat Nookaew,[2,5] Charles A. O'Brien,[2,3] and Melda Onal[1,2,6,*]

SUMMARY

Cre-mediated recombination is frequently used for cell type-specific loss of function (LOF) studies. A major limitation of this system is recombination in unwanted cell types. CRISPR interference (CRISPRi) has been used effectively for global LOF in mice. However, cell type-specific CRISPRi, independent of recombination-based systems, has not been reported. To test the feasibility of cell type-specific CRISPRi, we produced two novel knock-in mouse models that achieve gene suppression when used together: one expressing dCas9::KRAB under the control of a cell type-specific promoter and the other expressing a single guide RNA from a safe harbor locus. We then compared the phenotypes of mice in which the same gene was targeted by either CRISPRi or the Cre-loxP system, with cell specificity conferred by *Dmp1* regulatory elements in both cases. We demonstrate that CRISPRi is effective for cell type-specific LOF and that it provides improved cell type-specificity compared to the Cre-loxP system.

INTRODUCTION

Cell type-specific loss of function (LOF) studies have been the cornerstone of skeletal research since the development of Cre-driver strains that target bone-forming osteoblasts and bone-resorbing osteoclasts. Since the early 2000s, various Cre-driver strains that target different stages of the osteoblast lineage were produced by placing Cre expression under the control of cell type-specific gene regulatory elements.[1–11] However, it has been difficult to identify any genes that are expressed exclusively in a single cell type. In fact, most genes thought to be cell-type specific are also expressed in several other cell types and tissues. For example, *Dmp1* and *Sost* are commonly referred to as osteocyte-specific genes.[12–17] Osteocytes, which differentiate from osteoblasts, are embedded in the bone matrix, and orchestrate bone resorption and formation. We and others have used transcriptional regulatory elements of the *Dmp1* and *Sost* genes to produce Dmp1-Cre and Sost-Cre mouse strains.[6,8–11] However, it is now clear that these two genes are also expressed in several additional cell types in bone and other tissues, albeit at lower levels.[18–21] Accordingly, analysis of the cell types targeted by the Dmp1-Cre and Sost-Cre transgenes has shown that these Cre models are not as cell type-specific as once thought.[10,22–26] Specifically, while Sost-Cre is specific to osteocytes within the osteoblast lineage, it also recombines floxed alleles in hematopoietic cells.[10] On the other hand, Dmp1-Cre has been shown to recombine floxed alleles in additional cell types in bone, such as osteoblasts and Cxcl12-abundant reticular (CAR) cells,[22–26] and other tissues such as gastrointestinal mesenchymal cells.[22] Because gene inactivation in these other cell types may contribute to the observed phenotypes, it is essential to develop LOF models with improved cell type-specificity.

CRISPR interference (CRISPRi) is a recently developed approach to perform LOF.[27,28] This technique utilizes a catalytically inactive Cas9 (dCas9) fused to a transcriptional repressor domain to suppress target genes. The dCas9::repressor fusion protein is guided to a region within 100 bp flanking the transcriptional start site (TSS) of the target gene using a single guide RNA (sgRNA) complementary to that region.[29] Unlike the Cre-loxP system or the original CRISPR-Cas9 system, CRISPRi-based suppression does not cut or irreversibly modify the target DNA. Instead, CRISPRi-based LOF is achieved by inhibition of target gene transcription. *In vitro* studies have shown that the level of target gene suppression by CRISPRi is influenced by the location of the sgRNA relative to the TSS,[28,29] as well as the expression level of the system components, namely dCas9::KRAB and sgRNA.[27,30–32] We have recently demonstrated that a single transgene expressing CRISPRi components was able to globally suppress a target gene, *Tnfsf11*, *in vivo*.[33] We created transgenic mouse lines that expressed dCas9::KRAB and a *Tnfsf11* sgRNA ubiquitously and constitutively

[1]Department of Physiology and Cell Biology, University of Arkansas for Medical Sciences, Little Rock, AR 72205, USA

[2]Center for Musculoskeletal Disease Research (CMDR), University of Arkansas for Medical Sciences, Little Rock, AR 72205, USA

[3]Division of Endocrinology, University of Arkansas for Medical Sciences, Little Rock, AR 72205, USA

[4]Department of Biostatistics, University of Arkansas for Medical Sciences, Little Rock, AR 72205, USA

[5]Department of Biomedical Informatics, University of Arkansas for Medical Sciences, Little Rock, AR 72205, USA

[6]Lead contact

*Correspondence: monal@uams.edu

https://doi.org/10.1016/j.isci.2023.107428

but at varying levels (low, medium, and high). Comparison of these different lines showed that the level of *Tnfsf11* suppression correlated with the expression of the CRISPRi components. Specifically, high levels of dCas9::KRAB and sgRNA were required to suppress a target gene via CRISPRi. This is in contrast to what is observed with the Cre-loxP system, in which even low-level Cre expression can be sufficient to recombine floxed alleles, contributing to recombination in unwanted cell types.[34]

To allow for cell type-specific CRISPRi, a Cre-dependent dCas9::KRAB model, namely R26-LSL-dCas9-KRAB, has been created.[35] In this model, a transgene containing a CAG promoter followed by a loxP-stop-loxP (LSL) cassette and DNA encoding the dCas9::KRAB fusion protein was inserted into the Rosa safe harbor locus. Following Cre recombinase exposure, and in association with expression of a sgRNA at a different locus, this model can suppress expression of target genes. However, the cell type-specificity of this model is determined by the specificity of the Cre-driver strain used to delete the LSL cassette and, therefore, has the same lack of specificity as Cre-loxP models.

Based on the observed dose-dependence of CRISPRi that we observed previously, we hypothesized that expression of dCas9::KRAB under the control of transcriptional regulatory elements of a relatively cell type-specific gene would suppress targets only in cells that express high levels of that gene, thereby improving the specificity of LOF studies. While *Dmp1* is expressed by various cell types, its expression in osteocytes is much higher than in other cell types.[36,37] Based on this, we sought to determine if *Dmp1*-driven dCas9::KRAB would provide improved specificity compared to a Dmp1-Cre transgene. To test this, we performed LOF of a well-characterized gene (*Tnfsf11*) with both D*mp1*-driven Cre-loxP and D*mp1*-driven CRISPRi systems and compared the resultant phenotypes and specificity of *Tnfsf11* suppression.

RESULTS

Expression of a sgRNA from the *ROSA26* locus

Although expression of CRISPRi components via a single transgene can suppress target genes *in vivo*,[33] this approach requires production and screening of multiple founder lines for sufficient transgene expression for each new target. To avoid insertion site and copy number effects associated with transgenic approaches, and to facilitate efficient use of CRISPRi *in vivo*, we envisioned production of two murine models, each expressing one of the two CRISPRi components: one a knock-in model which expresses dCas9::KRAB and the other a knock-in model expressing one or more sgRNAs from a safe harbor locus.

Previous studies have shown that sgRNA expression level may be a limiting factor in target suppression by CRISPRi.[27,32] To determine if sgRNA expression from a safe harbor locus is sufficient for CRISPRi, we introduced a cassette expressing a *Tnfsf11* sgRNA into the murine *Rosa26* locus. We crossed the resulting mice, designated sgRNA^{Tnfsf11}, with mice that globally and constitutively express dCas9::KRAB, designated H11$^{dCas9::KRAB}$ [38,39] (Figure 1A). In mice hemizygous for both alleles, designated gCRi^{Tnfsf11}, ubiquitous expression of both CRISPRi components suppressed *Tnfsf11* in the bone, thymus, and spleen by more than 90% (Figure 1B).

Tnfsf11 encodes the TNF-family cytokine known as receptor activator of NF-κB ligand (RANKL). RANKL produced by cells of the mesenchymal lineage is necessary for the differentiation and survival of osteoclasts from myeloid progenitors.[23,40,41] Global suppression of *Tnfsf11* in gCRi^{Tnfsf11} mice decreased osteoclast formation to a level equivalent to deletion of *Tnfsf11* from the mouse genome (*Tnfsf11* KO mice), as indicated by the profoundly reduced expression of the osteoclast marker genes *CtsK* and *Acp5* (Figure 1C). Similar to what is observed in *Tnfsf11* KO mice, lack of osteoclasts in gCRi^{Tnfsf11} mice caused osteopetrosis indicated by high bone mass, lack of tooth eruption, and misshapen bones (Figures 1D and 1E). Independent of its role in osteoclast formation and survival, *Tnfsf11* is also required for lymph node formation.[41] CRISPRi-mediated *Tnfsf11* suppression was also sufficient to prevent lymph node development in gCRi^{Tnfsf11} mice (Figure 1F). Together, these results demonstrate that mice hemizygous for sgRNA^{Tnfsf11} express sgRNA at sufficient levels to potently suppress a target gene in the presence of dCas9::KRAB.

Conditional deletion of *Tnfsf11* versus suppression of *Tnfsf11* via CRISPRi

We next determined whether dCas9::KRAB expression from the endogenous *Dmp1* locus is sufficient, together with expression of the sgRNA from the Rosa26 locus, for CRISPRi. To do this, we inserted a dCas9::KRAB coding sequence into the endogenous *Dmp1* locus-producing Dmp1$^{dCas9::KRAB}$ mice. We selected *Dmp1* to drive dCas9::KRAB expression because this gene is expressed at high levels in

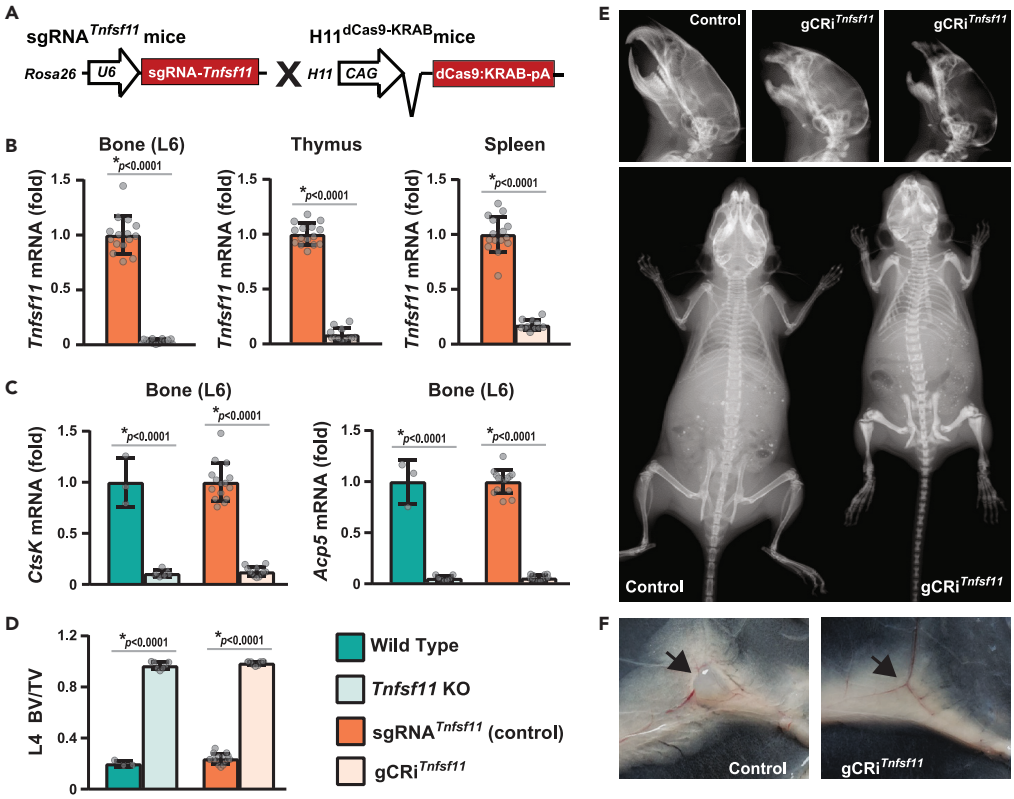

Figure 1. Global suppression of *Tnfsf11* using CRISPRi causes osteopetrosis

(A) sgRNA^{Tnfsf11} mice were crossed with H11$^{dCas9\text{-}KRAB}$ mice to globally suppress *Tnfsf11*.

(B–F) Gene expression and skeletal analysis of *Tnfsf11* knock-out mice (*Tnfsf11* KO, n = 7), their wild type littermates (n = 3); H11$^{dCas9\text{-}KRAB}$; sgRNA^{Tnfsf11} mice (gCRi^{Tnfsf11}, n = 12), and their littermate controls (sgRNA^{Tnfsf11} or Control, n = 15) were performed at 5 weeks of age. Both sexes were included. B, *Tnfsf11* mRNA levels were measured in the bone (lumbar vertebrae 6, L6), thymus, and spleen of gCRi^{Tnfsf11} mice and their littermate controls by quantitative real-time PCR (qRT-PCR). *p < 0.0001 as calculated by unpaired *t*-test with Welch's correction (L6 and spleen), or by Rank-Sum test (thymus). Data presented as mean ± standard deviation (SD). C, *CtsK* and *Acp5* mRNA levels were measured in bones of *Tnfsf11* KO, gCRi^{Tnfsf11} mice, and their littermate controls by qRT-PCR. For all qRT-PCR analyses, mRNA levels were normalized to mouse *Actb* and indicated as fold (normalized to the mean of the corresponding littermate control values). D, Vertebral cancellous bone volume over tissue volume (BV/TV) of *Tnfsf11* KO mice, gCRi^{Tnfsf11} mice and their littermate controls were measured by μCT analysis of lumbar vertebra 4 (L4). C and D, Data presented as mean ± SD, *p < 0.0001 comparing *Tnfsf11* KO or gCRi^{Tnfsf11} to their corresponding littermates; #p < 0.05 comparing wild type to sgRNA, or *Tnfsf11* KO to gCRi^{Tnfsf11} as assessed by one-way ANOVA with Tukey adjustment. E, Skull and whole body X-ray images were generated at five weeks of age. F, Arrows point to the presence or lack of inguinal lymph nodes in the control and gCRi^{Tnfsf11} mouse images. Data presented as mean + SD.

osteocytes.[12,36,37] To suppress *Tnfsf11* in osteocytes, we crossed the Dmp1$^{dCas9::KRAB}$ mice with sgRNA^{Tnfsf11} mice. Dmp1$^{dCas9::KRAB}$;sgRNA^{Tnfsf11} (Ot-CRi^{Tnfsf11}) mice and their littermate controls (wild type, Dmp1$^{dCas9::KRAB}$, and sgRNA^{Tnfsf11}) were born at expected mendelian ratios and were grossly indistinguishable from one another (Figure S1A).

At 6 months of age, microCT analysis was used to compare the skeletal phenotypes of mice whose *Tnfsf11* gene was inactivated using *Dmp1*-driven Cre-loxP deletion (Dmp1-Cre;Tnfsf11 $^{fl/fl}$) to mice whose *Tnfsf11* expression was suppressed using *Dmp1*-driven CRISPRi (Ot-CRi^{Tnfsf11}) (Figure 2; Figures S1B and S1C). The skeletal phenotype of Dmp1$^{dCas9::KRAB}$ or sgRNA^{Tnfsf11} hemizygous mice was indistinguishable from wild-type littermates suggesting that expression of dCas9::KRAB or the sgRNA alone does not alter bone mass (Figures 2B and 2C). While the magnitude of the effect was different, both *Tnfsf11* deletion and suppression increased cortical thickness (Figure 2B) and cancellous bone volume compared to littermate controls (Figure 2C). LOF of *Tnfsf11* by either system also led to similar architectural changes. Specifically, in both models, the increase in vertebral cancellous bone volume was associated with elevated trabecular number

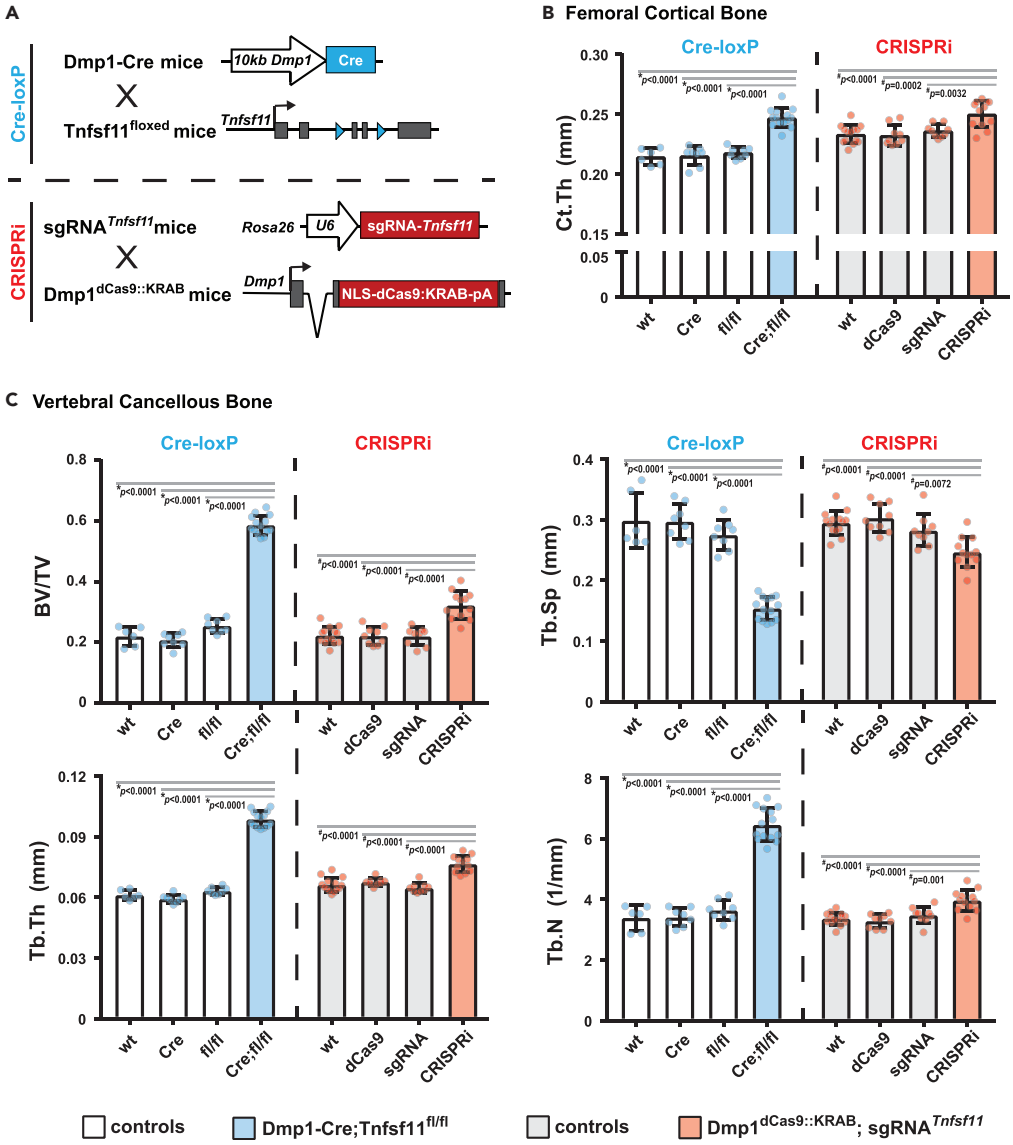

Figure 2. Comparison of *Tnfsf11* loss-of-function using *Dmp1*-driven Cre-loxP or *Dmp1*-driven CRISPRi

(A) Dmp1-Cre mice were crossed with Tnfsf11^{floxed} mice to create Dmp1-Cre;Tnfsf11$^{fl/fl}$ mice (Cre;fl/fl, blue bars) and their littermate controls (wild type [wt], Dmp1-Cre [Cre] and Tnfsf11$^{fl/fl}$ [fl/fl] mice, white bars). sgRNA^{Tnfsf11} mice were crossed with Dmp1$^{dCas9::KRAB}$ mice to produce Dmp1$^{dCas9::KRAB}$;sgRNA^{Tnfsf11} mice (CRISPRi, red bars) and their littermate controls (wild type [wt], Dmp1$^{dCas9::KRAB}$ [dCas9] and sgRNA^{Tnfsf11} [sgRNA] mice, light gray bars).

(B and C) The skeletal phenotype of 6-month-old female mice was compared by μCT analysis. B, Cortical thickness (Ct. Th) was measured at the femoral midshaft. C, Cancellous bone mass, and architecture were analyzed as bone volume over tissue volume (BV/TV), trabecular separation (Tb. Sp), trabecular thickness (Tb. Th), and trabecular number (Tb. N) in lumbar vertebrae 4. Data presented as mean ± SD. For deletion of *Tnfsf11* using Cre-loxP n = 6–14 mice/group; *p < 0.05 compared to each littermate control using one-way ANOVA with Tukey adjustment. For suppression of *Tnfsf11* using CRISPRi n = 9–14 mice/group; #, p < 0.05 compared to each littermate control using one-way ANOVA with Tukey adjustment. Individual Tukey p values for each comparison are provided in the graphs.

and thickness, and a resultant reduction in trabecular separation (Figure 2C). However, in both female and male mice, the high bone mass phenotype was more pronounced in mice whose *Tnfsf11* gene was deleted using *Dmp1*-Cre (Figures 2, S1B, and S1C). The difference in the magnitude of the skeletal changes may be due to greater cell type-specificity of the *Dmp1*-driven CRISPRi system, the fact that CRISPRi does not completely suppress target genes, or both.

Cell type specificity of *Dmp1*-driven CRISPRi

An optimal approach to compare the specificity of CRISPRi and Cre-loxP systems would be to target *Tnfsf11* with Dmp1-driven Cre-loxP or CRISPRi, and then use scRNA-seq to quantify *Tnfsf11* deletion or suppression in different cell types. However, in scRNA-seq, the barcoding and sequencing are performed on the 3′ or 5′ end of the mRNA transcripts. In *Tnfsf11*$^{fl/fl}$ mice, the exons flanked by *loxP* sites (exons 3 and 4) are near the middle of the transcript. Thus, the 3′ and 5′ ends of the *Tnfsf11* mRNA are still detectable in Dmp1-Cre;Tnfsf11$^{fl/fl}$ mice, even after Cre-mediated deletion of the floxed exons (data not shown). Due to this technical limitation, we could not use scRNA-seq to directly determine from which cell types Dmp1-Cre deletes *Tnfsf11*. As an alternative, we used a fluorescent Cre-reporter gene to determine which cell types were targeted by Dmp1-Cre and inferred that the floxed *Tnfsf11* allele was likely deleted from the same cell types when using Dmp1-Cre mice.

To do this, we marked all Dmp1-Cre targeted cells by activation of a Cre-reporter transgene and then examined whether *Dmp1*-driven CRISPRi suppressed *Tnfsf11* in any of the Cre-targeted cells. If CRISPRi targeted all of the cells targeted by Dmp1-Cre, then all of the reporter-positive cells that express *Tnfsf11* should show evidence of reduced *Tnfsf11* expression. If any Cre-targeted (reporter-positive) cells do not exhibit reduced *Tnfsf11* expression in the CRISPRi mice, then this would constitute evidence that the CRISPRi system targets a narrower range of cells. In other words, it is more cell-type-specific.

Dmp1-Cre, Ai9, Dmp1$^{dCas9::KRAB}$ mice were crossed with sgRNA^{Tnfsf11} mice to obtain Dmp1-Cre;Ai9;Dmp1$^{dCas9::KRAB}$;sgRNA^{Tnfsf11} mice (CRISPRi) and control littermates, Dmp1-Cre;Ai9;sgRNA^{Tnfsf11} (Control). Next, we isolated cells from femurs and tibias of CRISPRi and Control mice and sorted the Dmp1-Cre targeted cells by flow cytometry (Figure 3A). In this approach, Cre expression in both Control and CRISPRi mice activated the fluorescent Ai9 reporter. Therefore, in both Control and CRISPRi mice, cells targeted by Dmp1-Cre were TdTomato positive (Figure S2B). We then performed scRNA-seq of the tdTomato-positive cells isolated from each genotype to compare whether *Dmp1*-driven CRISPRi suppressed *Tnfsf11* in the same cell types targeted by Dmp1-Cre (Figures 3 and S2).

Previous studies have shown that the Dmp1-Cre transgene targets osteocytes, osteoblasts, and about 30% of CAR cells.[23,26,37] Consistent with these reports, our scRNA-seq analysis of sorted tdTomato-positive cells produced clusters corresponding to CAR cells (clusters 1 and 2), osteo-CAR cells (cluster 3), osteoblasts (clusters 4 and 5), and osteocytes (cluster 6) (Figures 3A and S2). OsteoCAR cells are a subset of CAR cells that express genes associated with osteoblast differentiation, although the relationship to either CAR cells or osteoblasts is uncertain.[42]

The endogenous *Dmp1* gene was highly expressed in osteocytes, with lower levels in osteoblasts and osteo-CAR cells (Figure 3B). Even though the Dmp1-Cre transgene led to activation of the reporter gene in CAR cells (Figure S2B), expression of the endogenous *Dmp1* gene was below the level of detection in most CAR cells. The reason for reporter expression in these cells is unclear but may result from low levels of Dmp1-Cre expression that are nonetheless sufficient for recombination or it may reflect the differentiation of osteo-CAR cells into CAR cells. We also cannot rule out the possibility that expression pattern of the Dmp1-Cre transgene is slightly different from that of the endogenous *Dmp1* gene. Be that as it may, the expression pattern of dCas9::KRAB mirrored that of the endogenous *Dmp1* gene (Figure 3B).

In Control mice, *Tnfsf11* transcripts were easily detected in CAR cells and some osteo-CAR cells as well as a small portion of osteoblasts and osteocytes (Figure 3B). Notably, *Dmp1*-driven CRISPRi had no impact on *Tnfsf11* expression in CAR cells or osteo-CAR cells (Figure 3B). In contrast, no *Tnfsf11* transcripts were detected in osteocytes in the *Dmp1*-driven CRISPRi mice (Figure 3B). Because the number of osteocytes expressing *Tnfsf11* in the control sample was so low, the significance of the lack of *Tnfsf11* transcripts in osteocytes of the CRISPRi sample is unclear, although it may reflect suppression by CRISPRi. Nonetheless, these results show that *Dmp1*-driven CRISPRi did not suppress *Tnfsf11* in CAR cells and osteo-CAR cells, whereas Dmp1-Cre recombination clearly occurs in these cell types. Thus, at least in the case of *Dmp1*-driven transgenes, the CRISPRi-based system targets a more restricted population of cells than the Cre-loxP system.

Dmp1-driven CRISPRi is functional up to 12 months of age

In CRISPRi, dCas9::KRAB has been proposed to facilitate transcriptional suppression of targets by both sterically blocking RNA polymerase binding and elongation, and by recruiting chromatin-modifying

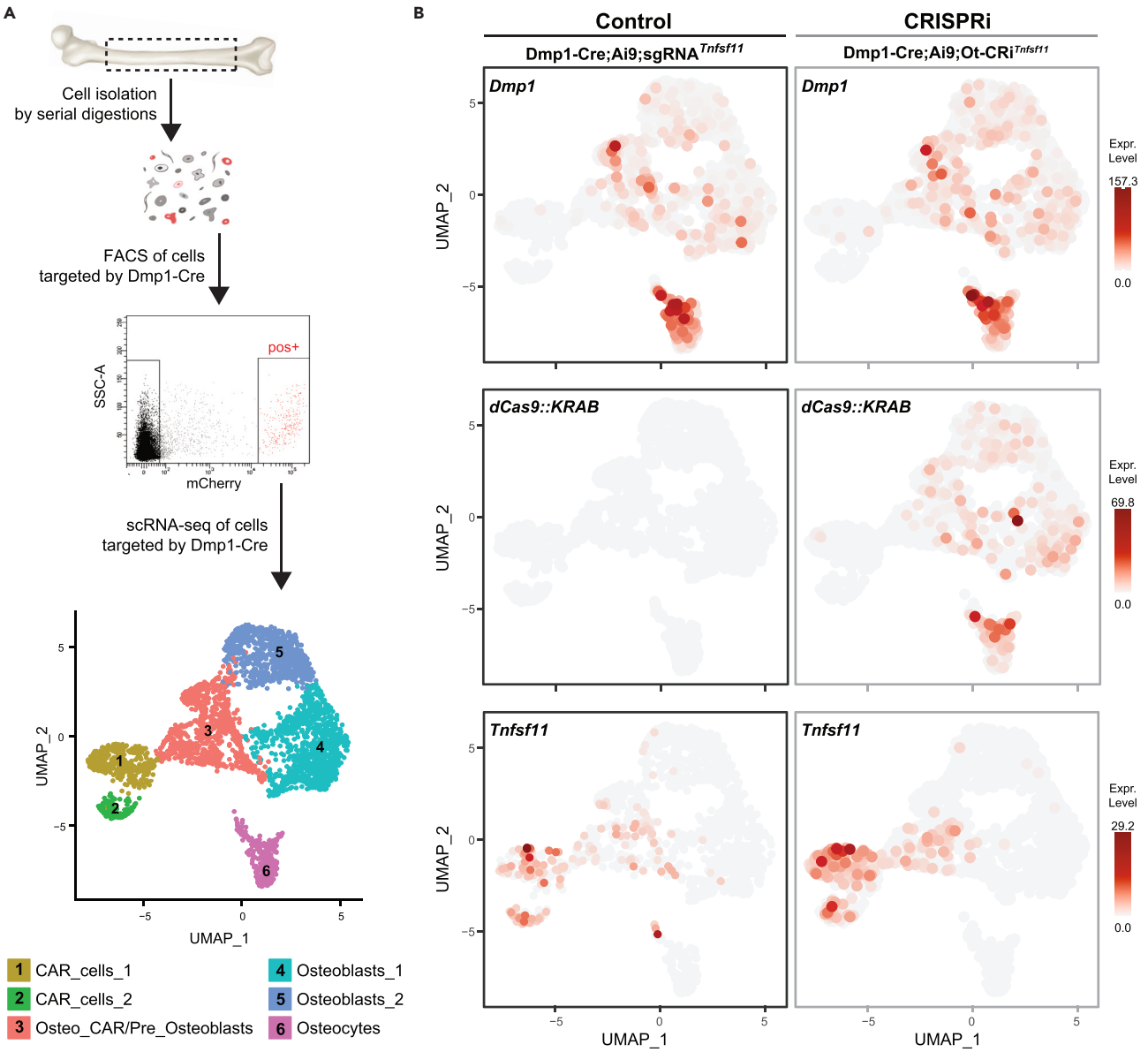

Figure 3. Specificity comparison of *Dmp1*-driven Cre-loxP or *Dmp1*-driven CRISPRi using scRNA-seq

(A) Femur and tibia shafts were subjected to serial digestions (see STAR Methods). Cells from fractions 2 to 8 were collected for flow cytometry. tdTomato-positive cells were sorted and used for scRNA-seq. Cell-clustering was performed using cluster-specific markers indicated in Figure S2.

(B) UMAP plot of cells showing *Dmp1* (top panel), *dCas9::KRAB* (middle panel), and *Tnfsf11* (bottom panel) expression in cells of control (Dmp1-Cre;Ai9;sgRNA^{Tnfsf11}) and CRISPRi (Dmp1-Cre;Ai9;Dmp1$^{dCas9::KRAB}$;sgRNA^{Tnfsf11} = Dmp1-Cre;Ai9;Ot-CRi^{Tnfsfs11}) mice.

complexes for epigenetic suppression.[27,28,38,43] Due to the temporal nature of these changes, target gene suppression by CRISPRi is reversible and is dependent on continuous expression of CRISPRi components. In our model, dCas9::KRAB transcription is controlled by *Dmp1* regulatory elements. An age-dependent decline in *Dmp1* expression has previously been reported.[44] Because a decline in *Dmp1* expression may translate to a reduction of dCas9::KRAB levels and a resultant decrease in target suppression, we determined if *Dmp1*-dependent *Tnfsf11* suppression persists in older mice. We examined the skeletal phenotype and target suppression of Dmp1$^{dCas9::KRAB}$;sgRNA^{Tnfsf11} (Ot-CRi^{Tnfsf11}) mice and their controls at 12 months of age. Bone mineral density (BMD) measurements at 4 and 12 months of age showed that Ot-CRi^{Tnfsf11} mice have higher BMD than controls at all sites examined (Figures 4A–4C). The skeletal phenotype caused by *Dmp1*-driven deletion of *Tnfsf11* becomes more pronounced as mice age.[45]

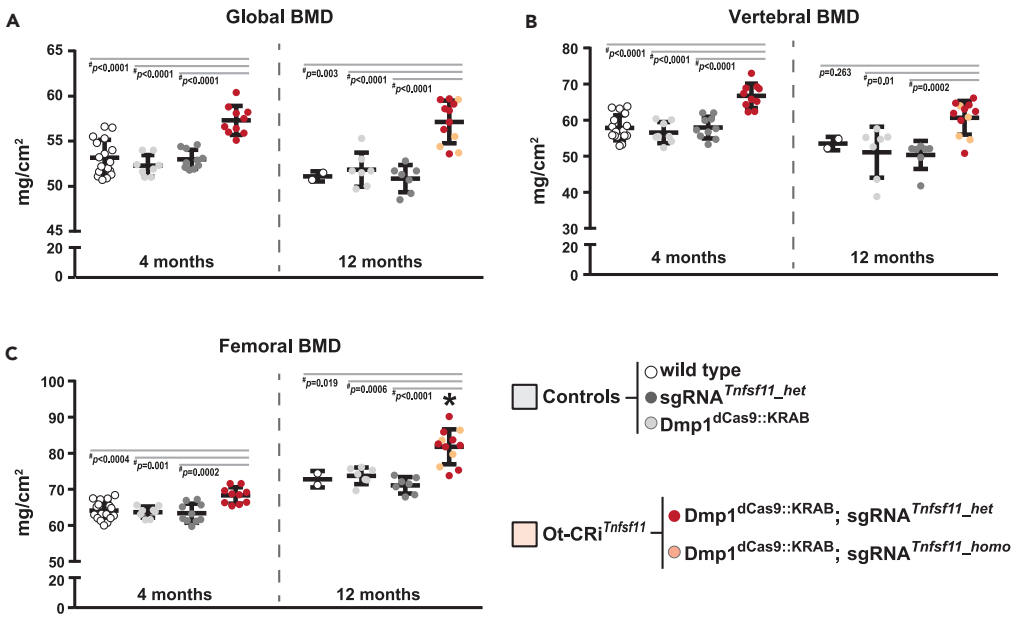

Figure 4. The phenotype of *Dmp1*-driven CRISPRi progresses with age

(A–C) BMD of female Dmp1$^{dCas9::KRAB}$;sgRNA^{Tnfsf11} mice (Ot-CRi^{Tnfsf11}) and their littermate controls (wild type, Dmp1$^{dCas9::KRAB}$, and sgRNA^{Tnfsf11} mice) were measured at 4 and 12 months of age. For the 4-month cohort n = 8–17 mice/group, and for the 12-month cohort n = 2–12 mice/group were used. Data presented as mean ± SD. For both ages #,p < 0.05 comparing Ot-CRi^{Tnfsf11} with each control group using one-way ANOVA with Tukey adjustment. Individual Tukey p values for each comparison are provided in the graphs.*, p < 0.05 for comparison of the change with age (between 12 and 4 months) for the Ot-CRi^{Tnfsf11} group and the change with age within the control groups using *t*-test (details explained in the Methods Statistics section).

Similarly, the increase in femoral BMD in Ot-CRi^{Tnfsf11} mice was more pronounced with age (Figure 4C). MicroCT measurements of 12-month-old Ot-CRi^{Tnfsf11} mice showed increased cancellous bone volume (Figures 5A–5D and S3A–S3D) and increased cortical thickness compared to controls (Figures 5E, 5F, S3E, and S3F). However, in both female and male mice, the high bone mass phenotype was more pronounced in mice whose *Tnfsf11* gene was deleted using Dmp1-Cre (Figures 5A–5F and S3).

Importantly, the high bone mass phenotype of both Dmp1-Cre;Tnsfs11 $^{fl/fl}$ and Ot-CRi^{Tnfsf11} mice were associated with *Tnfsf11* suppression (Figure 5G). As mentioned earlier, *Tnfsf11* is essential for the formation and survival of osteoclast.[41] We and others have shown that deletion of *Tnfsf11* from Dmp1-Cre targeted cells reduces osteoclast number, demonstrating that Dmp1-targeted cells support osteoclastogenesis by producing RANKL.[23,40] As expected, the lower *Tnfsf11* levels observed in both Dmp1-driven CRISPRi and Cre-loxP models reduced osteoclasts as evidenced by a decline in osteoclast-specific gene expression (Figure 5H and 5I). Together, these results demonstrate that target gene suppression by *Dmp1*-driven CRISPRi persists up to at least 12 months of age in both female and male mice.

DISCUSSION

Here we demonstrate that expression of a sgRNA and dCas9::KRAB from hemizygous safe harbor loci provides global LOF of target genes at a level comparable to that obtained by traditional knockout methodologies. We also show that CRISPRi can be used for cell type-specific LOF studies and that it may provide improved cell type-specificity over the Cre-loxP system. Our studies also set the stage for determining whether CRISPRi can be utilized for temporal, spatial, and progenitor-specific control of gene expression, as well as simultaneous cell type-specific suppression of multiple genes.

We previously showed effective global suppression of *Tnfsf11* using CRISPRi via a single transgene. However, significant animal-to-animal variation in the skeletal phenotype was observed within a given transgenic line in that study. Specifically, while most mice exhibited osteopetrosis, some exhibited partial formation of the femoral marrow cavity and partial tooth eruption.[33] These variations were likely due to

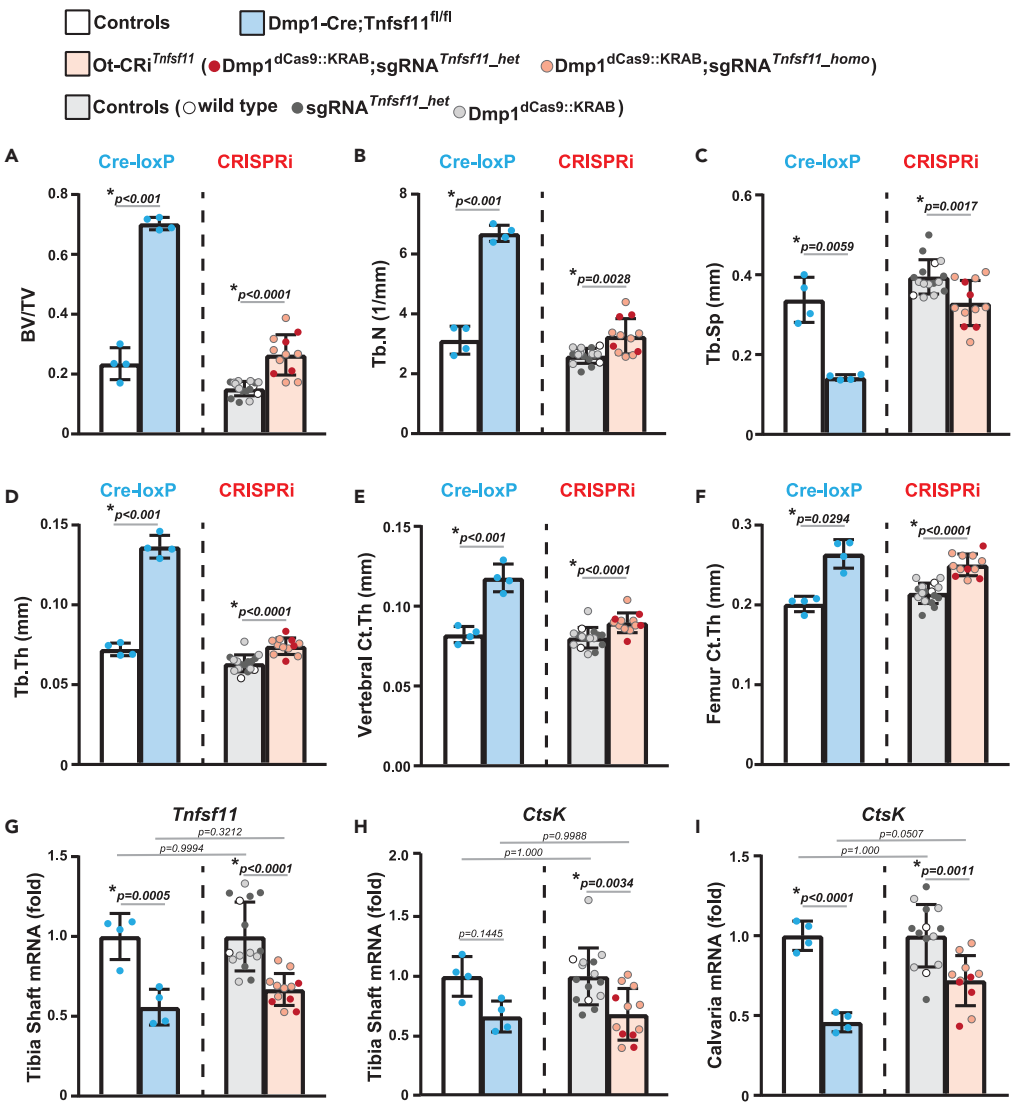

Figure 5. *Dmp1*-driven CRISPRi of *Tnfsf11* persists up to 12 months of age

The skeletal phenotype of 12-month-old female mice was compared by μCT analysis. For Cre-loxP, blue bars represent Dmp1-Cre;Tnfsf11$^{fl/fl}$ mice (blue bars, n = 4) and white bars represent their littermate controls (n = 4). For CRISPRi, pink bars represent Ot-CRi^{Tnfsf11} mice (n = 12), while the light gray bars represent their littermate controls (n = 15).

(A–D) Cancellous bone mass and architecture were analyzed as bone volume over tissue volume (BV/TV), trabecular separation (Tb. Sp), trabecular thickness (Tb. Th), and trabecular number (Tb. N) in lumbar vertebrae 4 (L4).

(E and F) Cortical thickness (Ct. Th) was measured in L4 (E) and femur (F). A–F, For the samples that have a normal distribution, *, $p < 0.05$ comparing Dmp1-Cre;Tnfsf11$^{fl/fl}$ or Ot-CRi^{Tnfsf11} to their own littermate controls using *t*-test. For the samples that did not have a normal distribution, namely BV/TV of CRi and femur Ct.Th, Rank-sum was used for comparison. Individual Tukey p values for each comparison are provided in the graphs.

(G–I) *Tnfsf11*(*G*) and *CtsK* (H and I) mRNA levels were measured in tibia shafts (G and H) and calvaria (I) of 12-month-old Dmp1-Cre;Tnfsf11$^{fl/fl}$ mice, Ot-CRi^{Tnfsf11} mice and their corresponding littermate controls by qRT-PCR. For all qRT-PCR analyses, mRNA levels were normalized to mouse *Mrsp2*. G-I, n = 4–15 mice/group; *, $p < 0.05$ comparing Dmp1-Cre;Tnfsf11$^{fl/fl}$ mice, Ot-CRi^{Tnfsf11} mice and their corresponding littermate controls; #, $p < 0.05$ comparing Dmp1-Cre;Tnfsf11$^{fl/fl}$ to Ot-CRi^{Tnfsf11}, or comparing controls using one-way Anova with Tukey adjustment. Individual Tukey p values for each comparison are provided in the graphs. All data presented as mean ± SD.

variable transgene expression stemming from the integration site. To avoid this possibility, in the present study, we globally suppressed *Tnfsf11* using knock-in mice that express the sgRNA and dCas9::KRAB from safe harbor loci. All mice with global *Tnfsf11* suppression exhibited osteopetrosis and lack of tooth eruption in the current study (Figure S4). Moreover, unlike our previous transgene-based CRISPRi, the

magnitude of osteoclast inhibition in gCRi^{Tnfsf11} mice was comparable to that observed in *Tnfsf11* null mice. These results suggest that the expression of CRISPRi components from safe harbor loci provides improved consistency over transgenic approaches for LOF studies.

Evidence presented here suggests that CRISPRi-based cell type-specific LOF studies provide improved cell type specificity compared with the Cre-loxP system. Specifically, using scRNA-seq analysis we show that two cell types targeted by Dmp1-Cre, namely CAR and Osteo_CAR cells, are not targets of *Dmp1*-driven CRISPRi. The different methodologies that were used to produce *Dmp1*-driven Cre-loxP and CRISPRi systems may have contributed to this difference in cell type specificity. Specifically, all currently available Dmp1-Cre driver strains are transgenic mice[6,8,9] in which Cre expression is driven by a 10kb or 8kb *Dmp1* promoter. In contrast, in our *Dmp1*-driven CRISPRi model, dCas9::KRAB is inserted into the endogenous *Dmp1* locus, and its expression is mediated by endogenous *Dmp1* regulatory elements. Therefore, the expression pattern of dCas9::KRAB may mirror that of the endogenous *Dmp1* gene better than Dmp1-Cre transgenes. However, we expect *Dmp1*-driven CRISPRi would also be more specific compared to a knock-in Dmp1-Cre model. Specifically, we show that *Dmp1*-driven CRISPRi does not alter *Tnfsf11* expression in Osteo_CAR cells. As endogenous *Dmp1* expression is detected in Osteo_CAR cells, it is reasonable to expect Cre expression and activity in Osteo_CAR cells even if the Cre coding sequence was knocked into the endogenous *Dmp1* locus. Because Osteo_CAR cells are targets of Dmp1-Cre, but they are not targeted by Dmp1-driven CRISPRi, Dmp1-driven CRISPRi appears to be more specific compared to the Dmp1-driven Cre-mediated recombination.

Previous *in vitro* studies show that upon cessation of dCas9::KRAB production, target gene suppression is reversed.[31,46] While the length of time required for target expression to return to baseline varies based on the target gene or reporter, for most targets tested 5 to 8 days is sufficient for full reversal.[31,46] Herein, we showed that suppression of *Tnfsf11* by the *Dmp1*-CRISPRi system persists at levels comparable to Cre-loxP even at 12 months of age (Figure 5G). However, it is possible that if *Dmp1* expression, and hence dCas9::KRAB expression, declines significantly as mice age further, the level of target knockdown may decrease. Therefore, future models may benefit from the use of newer systems such as CRISPRoff,[46] which utilizes a combination of ZNF10 KRAB, Dnmt3A, and Dnmt3L protein domains fused to dCas9, to epigenetically suppress targets in a manner stronger and more persistent than dCas9::KRAB alone.

Even with its current limitations, cell type-specific CRISPRi provides significant advantages over current recombination-mediated approaches. Perhaps one of the most useful is that LOF mice can be produced in a single cross. Deletion of loxP-flanked alleles requires two crosses: the first to introduce the Cre driver allele into the loxP-containing mice and the second to produce mice homozygous for the loxP-flanked allele. Targeting multiple loci simultaneously can require several additional crosses. Therefore, the time and cost savings gained by producing mice with a single cross can be substantial. It is also important to consider that introduction of new sgRNA expression cassettes into safe-harbor loci requires significantly less time and money than creating new loxP-flanked alleles using traditional gene targeting in embryonic stem cells. Thus, even though the number of mouse lines expressing sgRNAs is currently much lower than the number of loxP-flanked alleles, production of new sgRNA mice should be relatively efficient.

Further development and improvement of cell type-specific CRISPRi systems has the potential to provide several benefits in addition to improvement of cell type specificity. For example, while tetracycline- or tamoxifen-regulated Cre strains are available to perform temporally controlled cell-type-specific LOF studies, one limitation of these systems is their leakiness (inducer-independent expression of Cre expression at low levels). However, because CRISPRi is dose-dependent and requires high-level expression of system components for target gene suppression, if dCas9::KRAB is expressed under the control of a tetracycline-regulated cell type-specific promoter, low-level ligand-independent expression of dCas9::KRAB would likely not be sufficient for the suppression of target genes. Moreover, the reversible nature of CRISPRi can also be utilized to target LOF specifically to progenitor cells within a given lineage. To accomplish this, dCas9::KRAB expression can be placed under the control of progenitor-specific promoters that are not expressed in cells at later stages of the lineage.

We do not anticipate that the use of CRISPRi will completely replace recombination-based LOF approaches. Instead, CRISPRi can be used as an adjunct approach to answer questions that cannot be addressed using recombination-based gene inactivation. Perhaps the most significant limitation of recombination-based systems is the lack of truly cell-type-specific Cre driver strains. Here we present evidence that

CRISPRi can produce gene suppression that is more cell type-specific than Cre-mediated recombination. Furthermore, the potential to suppress genes specifically in progenitor cells is something that is not possible with recombination-based LOF. In our view, these advantages warrant continued development of CRISPRi for LOF studies.

Limitations of the study

One limitation of our study is that it was not possible to directly measure the efficacy of *Tnfsf11* suppression in osteocytes of the *Dmp1*-driven CRISPRi mice. Nonetheless, the reduction in osteoclasts and increase in bone mass in the *Dmp1*-driven CRISPRi mice were lower in magnitude compared to that achieved by Dmp1-Cre mediated *Tnfsf11* deletion (Figures 2 and 5). There are multiple potential explanations for this difference. First, the stronger phenotype in Dmp1-Cre mice may be due to loss of *Tnfsf11* function in a broader range of cell types than in the *Dmp1*-driven CRISPRi mice. Our scRNA-seq results are consistent with this possibility. Second, it is possible that *Dmp1*-driven *Tnfsf11* suppression in osteocytes did not completely eliminate *Tnfsf11* production in these cells, whereas Dmp1-Cre mediated deletion did. Global dCas9::KRAB expression using a strong promoter was capable of suppressing *Tnfsf11* to a level that mimicked gene deletion. However, it is possible that *Dmp1*-driven dCas9::KRAB expression was not as effective. Future studies will examine whether sgRNA or dCas9::repressor domain can be modified to increase the potency of suppression. Such modifications may include the use of (i) multiple sgRNAs for the same target gene, (ii) alternative sgRNA design that improves sgRNA stability and sgRNA-dCas9 assembly,[47] (iii) bipartite repressor domains such as KRAB-MeCP2,[48] or (iv) more potent KRAB domains such as ZIM3 KRAB domain.[49]

STAR★METHODS

Detailed methods are provided in the online version of this paper and include the following:

- KEY RESOURCES TABLE
- RESOURCE AVAILABILITY
  - Lead contact
  - Materials availability
  - Data and code availability
- EXPERIMENTAL MODEL AND SUBJECT DETAILS
  - Generation of mice
  - Murine models
- METHOD DETAILS
  - RNA isolation and gene expression analysis
  - Skeletal analysis
  - scRNA-seq sample preparation
  - scRNA-seq data analysis
- QUANTIFICATION AND STATISTICAL ANALYSIS

SUPPLEMENTAL INFORMATION

Supplemental information can be found online at https://doi.org/10.1016/j.isci.2023.107428.

ACKNOWLEDGMENTS

This work was supported by the National Institute of Arthritis and Musculoskeletal and Skin Diseases (NIAMS) R21AR076575, National Institute of General Medical Sciences (NIGMS) grants P20GM125503, and the UAMS Bone and Joint Initiative. We thank the Genetic Models Core Facility for the production of the sgRNA murine model, the Bone Histology and Imaging Core for their help with tissue collection and analysis, the UAMS Genomics Core for their help with scRNA-seq, and the staff of the UAMS Department of Laboratory Animal Medicine for their help with husbandry and care of mice.

AUTHOR CONTRIBUTIONS

M.O. and C.A.O. designed murine models and experiments. Q.F. helped with the design, production, and sequence identification of the sgRNA murine model. M.O., D.J.L., and N.S.A. performed experiments. M.O., D.J.L., N.S.A, J.A.C., and A.J. contributed to tissue collection. D.J.L., S.B.H., J.A.H., and A.J. performed μCT analysis. M.O., D.J.L., and N.S.A. performed gene expression analysis. T.J.D. performed

statistical analysis of data. I.N. performed bioinformatics analysis of the scRNA-seq. M.O. wrote the manuscript. All authors revised the manuscript.

DECLARATION OF INTERESTS

The authors declare no competing interests.

INCLUSION AND DIVERSITY

We support inclusive, diverse, and equitable conduct of research.

Received: December 16, 2022
Revised: June 12, 2023
Accepted: July 17, 2023
Published: July 20, 2023

REFERENCES

1. Zhang, M., Xuan, S., Bouxsein, M.L., von Stechow, D., Akeno, N., Faugere, M.C., Malluche, H., Zhao, G., Rosen, C.J., Efstratiadis, A., and Clemens, T.L. (2002). Osteoblast-specific knockout of the insulin-like growth factor (IGF) receptor gene reveals an essential role of IGF signaling in bone matrix mineralization. J. Biol. Chem. *277*, 44005–44012. https://doi.org/10.1074/jbc.M208265200.

2. Logan, M., Martin, J.F., Nagy, A., Lobe, C., Olson, E.N., and Tabin, C.J. (2002). Expression of Cre Recombinase in the developing mouse limb bud driven by a Prxl enhancer. Genesis *33*, 77–80. https://doi.org/10.1002/gene.10092.

3. Dacquin, R., Starbuck, M., Schinke, T., and Karsenty, G. (2002). Mouse alpha1(I)-collagen promoter is the best known promoter to drive efficient Cre recombinase expression in osteoblast. Dev. Dyn. *224*, 245–251. https://doi.org/10.1002/dvdy.10100.

4. Kim, J.E., Nakashima, K., and de Crombrugghe, B. (2004). Transgenic mice expressing a ligand-inducible cre recombinase in osteoblasts and odontoblasts: a new tool to examine physiology and disease of postnatal bone and tooth. Am. J. Pathol. *165*, 1875–1882. https://doi.org/10.1016/S0002-9440(10)63240-3.

5. Rodda, S.J., and McMahon, A.P. (2006). Distinct roles for Hedgehog and canonical Wnt signaling in specification, differentiation and maintenance of osteoblast progenitors. Development *133*, 3231–3244. https://doi.org/10.1242/dev.02480.

6. Lu, Y., Xie, Y., Zhang, S., Dusevich, V., Bonewald, L.F., and Feng, J.Q. (2007). DMP1-targeted Cre expression in odontoblasts and osteocytes. J. Dent. Res. *86*, 320–325. https://doi.org/10.1177/154405910708600404.

7. Zha, L., Hou, N., Wang, J., Yang, G., Gao, Y., Chen, L., and Yang, X. (2008). Collagen1alpha1 promoter drives the expression of Cre recombinase in osteoblasts of transgenic mice. J Genet Genomics *35*, 525–530. https://doi.org/10.1016/S1673-8527(08)60072-7.

8. Powell, W.F., Jr., Barry, K.J., Tulum, I., Kobayashi, T., Harris, S.E., Bringhurst, F.R., and Pajevic, P.D. (2011). Targeted ablation of the PTH/PTHrP receptor in osteocytes impairs bone structure and homeostatic calcemic responses. J. Endocrinol. *209*, 21–32. https://doi.org/10.1530/JOE-10-0308.

9. Bivi, N., Condon, K.W., Allen, M.R., Farlow, N., Passeri, G., Brun, L.R., Rhee, Y., Bellido, T., and Plotkin, L.I. (2012). Cell autonomous requirement of connexin 43 for osteocyte survival: consequences for endocortical resorption and periosteal bone formation. J. Bone Miner. Res. *27*, 374–389. https://doi.org/10.1002/jbmr.548.

10. Xiong, J., Piemontese, M., Onal, M., Campbell, J., Goellner, J.J., Dusevich, V., Bonewald, L., Manolagas, S.C., and O'Brien, C.A. (2015). Osteocytes, not Osteoblasts or Lining Cells, are the Main Source of the RANKL Required for Osteoclast Formation in Remodeling Bone. PLoS One *10*, e0138189. https://doi.org/10.1371/journal.pone.0138189.

11. Maurel, D.B., Matsumoto, T., Vallejo, J.A., Johnson, M.L., Dallas, S.L., Kitase, Y., Brotto, M., Wacker, M.J., Harris, M.A., Harris, S.E., and Bonewald, L.F. (2019). Characterization of a novel murine Sost ER(T2) Cre model targeting osteocytes. Bone Res. *7*, 6. https://doi.org/10.1038/s41413-018-0037-4.

12. Toyosawa, S., Shintani, S., Fujiwara, T., Ooshima, T., Sato, A., Ijuhin, N., and Komori, T. (2001). Dentin matrix protein 1 is predominantly expressed in chicken and rat osteocytes but not in osteoblasts. J. Bone Miner. Res. *16*, 2017–2026. https://doi.org/10.1359/jbmr.2001.16.11.2017.

13. Fen, J.Q., Zhang, J., Dallas, S.L., Lu, Y., Chen, S., Tan, X., Owen, M., Harris, S.E., and MacDougall, M. (2002). Dentin matrix protein 1, a target molecule for Cbfa1 in bone, is a unique bone marker gene. J. Bone Miner. Res. *17*, 1822–1831. https://doi.org/10.1359/jbmr.2002.17.10.1822.

14. Kalajzic, I., Braut, A., Guo, D., Jiang, X., Kronenberg, M.S., Mina, M., Harris, M.A., Harris, S.E., and Rowe, D.W. (2004). Dentin matrix protein 1 expression during osteoblastic differentiation, generation of an osteocyte GFP-transgene. Bone *35*, 74–82. https://doi.org/10.1016/j.bone.2004.03.006.

15. Brunkow, M.E., Gardner, J.C., Van Ness, J., Paeper, B.W., Kovacevich, B.R., Proll, S., Skonier, J.E., Zhao, L., Sabo, P.J., Fu, Y., et al. (2001). Bone dysplasia sclerosteosis results from loss of the SOST gene product, a novel cystine knot-containing protein. Am. J. Hum. Genet. *68*, 577–589. https://doi.org/10.1086/318811.

16. Balemans, W., Ebeling, M., Patel, N., Van Hul, E., Olson, P., Dioszegi, M., Lacza, C., Wuyts, W., Van Den Ende, J., Willems, P., et al. (2001). Increased bone density in sclerosteosis is due to the deficiency of a novel secreted protein (SOST). Hum. Mol. Genet. *10*, 537–543. https://doi.org/10.1093/hmg/10.5.537.

17. van Bezooijen, R.L., Roelen, B.A.J., Visser, A., van der Wee-Pals, L., de Wilt, E., Karperien, M., Hamersma, H., Papapoulos, S.E., ten Dijke, P., and Löwik, C.W.G.M. (2004). Sclerostin is an osteocyte-expressed negative regulator of bone formation, but not a classical BMP antagonist. J. Exp. Med. *199*, 805–814. https://doi.org/10.1084/jem.20031454.

18. Magarò, M.S., Bertacchini, J., Florio, F., Zavatti, M., Potì, F., Cavani, F., Amore, E., De Santis, I., Bevilacqua, A., Reggiani Bonetti, L., et al. (2021). Identification of Sclerostin as a Putative New Myokine Involved in the Muscle-to-Bone Crosstalk. Biomedicines *9*, 71. https://doi.org/10.3390/biomedicines9010071.

19. Weivoda, M.M., Youssef, S.J., and Oursler, M.J. (2017). Sclerostin expression and functions beyond the osteocyte. Bone *96*, 45–50. https://doi.org/10.1016/j.bone.2016.11.024.

20. Yoshioka, H., Okita, S., Nakano, M., Minamizaki, T., Nubukiyo, A., Sotomaru, Y., Bonnelye, E., Kozai, K., Tanimoto, K., Aubin, J.E., and Yoshiko, Y. (2021). Single-Cell RNA-Sequencing Reveals the Breadth of Osteoblast Heterogeneity. JBMR Plus *5*, e10496. https://doi.org/10.1002/jbm4.10496.

21. Terasawa, M., Shimokawa, R., Terashima, T., Ohya, K., Takagi, Y., and Shimokawa, H. (2004). Expression of dentin matrix protein 1

(DMP1) in nonmineralized tissues. J. Bone Miner. Metab. *22*, 430–438. https://doi.org/10.1007/s00774-004-0504-4.

22. Lim, J., Burclaff, J., He, G., Mills, J.C., and Long, F. (2017). Unintended targeting of Dmp1-Cre reveals a critical role for Bmpr1a signaling in the gastrointestinal mesenchyme of adult mice. Bone Res. *5*, 16049. https://doi.org/10.1038/boneres.2016.49.

23. Xiong, J., Onal, M., Jilka, R.L., Weinstein, R.S., Manolagas, S.C., and O'Brien, C.A. (2011). Matrix-embedded cells control osteoclast formation. Nat. Med. *17*, 1235–1241. https://doi.org/10.1038/nm.2448.

24. Kalajzic, I., Matthews, B.G., Torreggiani, E., Harris, M.A., Divieti Pajevic, P., and Harris, S.E. (2013). In vitro and in vivo approaches to study osteocyte biology. Bone *54*, 296–306. https://doi.org/10.1016/j.bone.2012.09.040.

25. Lim, J., Shi, Y., Karner, C.M., Lee, S.Y., Lee, W.C., He, G., and Long, F. (2016). Dual function of Bmpr1a signaling in restricting preosteoblast proliferation and stimulating osteoblast activity in mouse. Development *143*, 339–347. https://doi.org/10.1242/dev.126227.

26. Zhang, J., and Link, D.C. (2016). Targeting of Mesenchymal Stromal Cells by Cre-Recombinase Transgenes Commonly Used to Target Osteoblast Lineage Cells. J. Bone Miner. Res. *31*, 2001–2007. https://doi.org/10.1002/jbmr.2877.

27. Qi, L.S., Larson, M.H., Gilbert, L.A., Doudna, J.A., Weissman, J.S., Arkin, A.P., and Lim, W.A. (2013). Repurposing CRISPR as an RNA-guided platform for sequence-specific control of gene expression. Cell *152*, 1173–1183. https://doi.org/10.1016/j.cell.2013.02.022.

28. Gilbert, L.A., Larson, M.H., Morsut, L., Liu, Z., Brar, G.A., Torres, S.E., Stern-Ginossar, N., Brandman, O., Whitehead, E.H., Doudna, J.A., et al. (2013). CRISPR-mediated modular RNA-guided regulation of transcription in eukaryotes. Cell *154*, 442–451. https://doi.org/10.1016/j.cell.2013.06.044.

29. Gilbert, L.A., Horlbeck, M.A., Adamson, B., Villalta, J.E., Chen, Y., Whitehead, E.H., Guimaraes, C., Panning, B., Ploegh, H.L., Bassik, M.C., et al. (2014). Genome-Scale CRISPR-Mediated Control of Gene Repression and Activation. Cell *159*, 647–661. https://doi.org/10.1016/j.cell.2014.09.029.

30. Fontana, J., Dong, C., Ham, J.Y., Zalatan, J.G., and Car, J.M. (2018). Regulated Expression of sgRNAs Tunes CRISPRi in E. coli. Biotechnol. J. *13*, e1800069. https://doi.org/10.1002/biot.201800069.

31. Mandegar, M.A., Huebsch, N., Frolov, E.B., Shin, E., Truong, A., Olvera, M.P., Chan, A.H., Miyaoka, Y., Holmes, K., Spencer, C.I., et al. (2016). CRISPR Interference Efficiently Induces Specific and Reversible Gene Silencing in Human iPSCs. Cell Stem Cell *18*, 541–553. https://doi.org/10.1016/j.stem.2016.01.022.

32. Wang, Y., Xie, Y., Dong, Z.C., Jiang, X.J., Gong, P., Lu, J., and Wan, F. (2021). [Levels of sgRNA as a Major Factor Affecting CRISPRi Knockdown Efficiency in K562 Cells]. Mol. Biol. *55*, 86–95. https://doi.org/10.31857/S0026898421010146.

33. MacLeod, R.S., Cawley, K.M., Gubrij, I., Nookaew, I., Onal, M., and O'Brien, C.A. (2019). Effective CRISPR interference of an endogenous gene via a single transgene in mice. Sci. Rep. *9*, 17312. https://doi.org/10.1038/s41598-019-53611-6.

34. Schmidt-Supprian, M., and Rajewsky, K. (2007). Vagaries of conditional gene targeting. Nat. Immunol. *8*, 665–668. https://doi.org/10.1038/ni0707-665.

35. Gemberling, M.P., Siklenka, K., Rodriguez, E., Tonn-Eisinger, K.R., Barrera, A., Liu, F., Kantor, A., Li, L., Cigliola, V., Hazlett, M.F., et al. (2021). Transgenic mice for in vivo epigenome editing with CRISPR-based systems. Nat. Methods *18*, 965–974. https://doi.org/10.1038/s41592-021-01207-2.

36. Zhong, L., Yao, L., Tower, R.J., Wei, Y., Miao, Z., Park, J., Shrestha, R., Wang, L., Yu, W., Holdreith, N., et al. (2020). Single cell transcriptomics identifies a unique adipose lineage cell population that regulates bone marrow environment. Elife *9*, e54695. https://doi.org/10.7554/eLife.54695.

37. Wang, J.S., Kamath, T., Mazur, C.M., Mirzamohammadi, F., Rotter, D., Hojo, H., Castro, C.D., Tokavanich, N., Patel, R., Govea, N., et al. (2021). Control of osteocyte dendrite formation by Sp7 and its target gene osteocrin. Nat. Commun. *12*, 6271. https://doi.org/10.1038/s41467-021-26571-7.

38. Lindtner, S., Catta-Preta, R., Tian, H., Su-Feher, L., Price, J.D., Dickel, D.E., Greiner, V., Silberberg, S.N., McKinsey, G.L., McManus, M.T., et al. (2019). Genomic Resolution of DLX-Orchestrated Transcriptional Circuits Driving Development of Forebrain GABAergic Neurons. Cell Rep. *28*, 2048–2063.e8. https://doi.org/10.1016/j.celrep.2019.07.022.

39. Yoneshiro, T., Wang, Q., Tajima, K., Matsushita, M., Maki, H., Igarashi, K., Dai, Z., White, P.J., McGarrah, R.W., Ilkayeva, O.R., et al. (2019). BCAA catabolism in brown fat controls energy homeostasis through SLC25A44. Nature *572*, 614–619. https://doi.org/10.1038/s41586-019-1503-x.

40. Nakashima, T., Hayashi, M., Fukunaga, T., Kurata, K., Oh-Hora, M., Feng, J.Q., Bonewald, L.F., Kodama, T., Wutz, A., Wagner, E.F., et al. (2011). Evidence for osteocyte regulation of bone homeostasis through RANKL expression. Nat. Med. *17*, 1231–1234. https://doi.org/10.1038/nm.2452.

41. Kong, Y.Y., Yoshida, H., Sarosi, I., Tan, H.L., Timms, E., Capparelli, C., Morony, S., Oliveira-dos-Santos, A.J., Van, G., Itie, A., et al. (1999). OPGL is a key regulator of osteoclastogenesis, lymphocyte development and lymph-node organogenesis. Nature *397*, 315–323. https://doi.org/10.1038/16852.

42. Baccin, C., Al-Sabah, J., Velten, L., Helbling, P.M., Grünschläger, F., Hernández-Malmierca, P., Nombela-Arrieta, C., Steinmetz, L.M., Trumpp, A., and Haas, S. (2020). Combined single-cell and spatial transcriptomics reveal the molecular, cellular and spatial bone marrow niche organization. Nat. Cell Biol. *22*, 38–48. https://doi.org/10.1038/s41556-019-0439-6.

43. Hilton, I.B., D'Ippolito, A.M., Vockley, C.M., Thakore, P.I., Crawford, G.E., Reddy, T.E., and Gersbach, C.A. (2015). Epigenome editing by a CRISPR-Cas9-based acetyltransferase activates genes from promoters and enhancers. Nat. Biotechnol. *33*, 510–517. https://doi.org/10.1038/nbt.3199.

44. Sato, S., Hashimoto, J., Usami, Y., Ohyama, K., Isogai, Y., Hagiwara, Y., Maruyama, N., Komori, T., Kuroda, T., and Toyosawa, S. (2013). Novel sandwich ELISAs for rat DMP1: age-related decrease of circulatory DMP1 levels in male rats. Bone *57*, 429–436. https://doi.org/10.1016/j.bone.2013.09.013.

45. Kim, H.N., Xiong, J., MacLeod, R.S., Iyer, S., Fujiwara, Y., Cawley, K.M., Han, L., He, Y., Thostenson, J.D., Ferreira, E., et al. (2020). Osteocyte RANKL is required for cortical bone loss with age and is induced by senescence. JCI Insight *5*, e138815. https://doi.org/10.1172/jci.insight.138815.

46. Nunez, J.K., Chen, J., Pommier, G.C., Cogan, J.Z., Replogle, J.M., Adriaens, C., Ramadoss, G.N., Shi, Q., Hung, K.L., Samelson, A.J., et al. (2021). Genome-wide programmable transcriptional memory by CRISPR-based epigenome editing. Cell *184*, 2503–2519.e2517. https://doi.org/10.1016/j.cell.2021.03.025.

47. Chen, B., Gilbert, L.A., Cimini, B.A., Schnitzbauer, J., Zhang, W., Li, G.W., Park, J., Blackburn, E.H., Weissman, J.S., Qi, L.S., and Huang, B. (2013). Dynamic imaging of genomic loci in living human cells by an optimized CRISPR/Cas system. Cell *155*, 1479–1491. https://doi.org/10.1016/j.cell.2013.12.001.

48. Yeo, N.C., Chavez, A., Lance-Byrne, A., Chan, Y., Menn, D., Milanova, D., Kuo, C.C., Guo, X., Sharma, S., Tung, A., et al. (2018). An enhanced CRISPR repressor for targeted mammalian gene regulation. Nat. Methods *15*, 611–616. https://doi.org/10.1038/s41592-018-0048-5.

49. Alerasool, N., Segal, D., Lee, H., and Taipale, M. (2020). An efficient KRAB domain for CRISPRi applications in human cells. Nat. Methods *17*, 1093–1096. https://doi.org/10.1038/s41592-020-0966-x.

50. Xiong, J., Cawley, K., Piemontese, M., Fujiwara, Y., Zhao, H., Goellner, J.J., and O'Brien, C.A. (2018). Soluble RANKL contributes to osteoclast formation in adult mice but not ovariectomy-induced bone loss. Nat. Commun. *9*, 2909. https://doi.org/10.1038/s41467-018-05244-y.

51. Chu, V.T., Weber, T., Graf, R., Sommermann, T., Petsch, K., Sack, U., Volchkov, P., Rajewsky, K., and Kühn, R. (2016). Efficient generation of Rosa26 knock-in mice using CRISPR/Cas9 in C57BL/6 zygotes. BMC Biotechnol. *16*, 4. https://doi.org/10.1186/s12896-016-0234-4.

52. Livak, K.J., and Schmittgen, T.D. (2001). Analysis of relative gene expression data using real-time quantitative PCR and the 2(-Delta Delta C(T)) Method. Methods *25*, 402–408. https://doi.org/10.1006/meth.2001.1262.

53. Akel, N., MacLeod, R.S., Berryhill, S.B., Laster, D.J., Dimori, M., Crawford, J.A., Fu, Q., and Onal, M. (2022). Loss of chaperone-mediated autophagy is associated with low vertebral cancellous bone mass. Sci. Rep. *12*, 3134. https://doi.org/10.1038/s41598-022-07157-9.

54. Piemontese, M., Almeida, M., Robling, A.G., Kim, H.N., Xiong, J., Thostenson, J.D., Weinstein, R.S., Manolagas, S.C., O'Brien, C.A., and Jilka, R.L. (2017). Old age causes de novo intracortical bone remodeling and porosity in mice. JCI Insight *2*, e93771. https://doi.org/10.1172/jci.insight.93771.

55. Bouxsein, M.L., Boyd, S.K., Christiansen, B.A., Guldberg, R.E., Jepsen, K.J., and Müller, R. (2010). Guidelines for assessment of bone microstructure in rodents using micro-computed tomography. J. Bone Miner. Res. *25*, 1468–1486. https://doi.org/10.1002/jbmr.141.

56. Stuart, T., Butler, A., Hoffman, P., Hafemeister, C., Papalexi, E., Mauck, W.M., 3rd, Hao, Y., Stoeckius, M., Smibert, P., and Satija, R. (2019). Comprehensive Integration of Single-Cell Data. Cell *177*, 1888–1902.e21. https://doi.org/10.1016/j.cell.2019.05.031.

57. Blondel, V.D., Guillaume, J.-L., Lambiotte, R., and Lefebvre, E. (2008). Fast unfolding of communities in large networks. J. Stat. Mech. *2008*, P10008. https://doi.org/10.1088/1742-5468/2008/10/p10008.

58. Finak, G., McDavid, A., Yajima, M., Deng, J., Gersuk, V., Shalek, A.K., Slichter, C.K., Miller, H.W., McElrath, M.J., Prlic, M., et al. (2015). MAST: a flexible statistical framework for assessing transcriptional changes and characterizing heterogeneity in single-cell RNA sequencing data. Genome Biol. *16*, 278. https://doi.org/10.1186/s13059-015-0844-5.

STAR★METHODS

KEY RESOURCES TABLE

REAGENT or RESOURCE	SOURCE	IDENTIFIER
Chemicals, peptides, and recombinant proteins		
Trizol Reagent	Life Technologies	Cat No: 15596018
RNAeasy Plus Mini Kit	Qiagen	Cat No: 74136
High-Capacity cDNA Reverse Transcription Kit	Applied Biosystems	Cat No: 4368814
TaqMan Fast Advanced Master Mix	Applied Biosystems	Cat No: 4444964
HBSS	Gibco	Cat No: 14025-076
PBS	Gibco	Cat No: 21600010
EDTA	Invitrogen	Cat No: 15575-020
LiberaseTM	Roche, Sigma	Cat No: LIBTM-RO
Deposited data		
scRNA-seq data files	This paper	BioProject PRJNA896097
Experimental models: Organisms/strains		
Mouse: *B6.129-Tnfsf11*$^{tm1.1Caob}$*/J*	The Jackson Laboratory	Strain #:018978, RRID:IMSR_JAX:018978
Mouse: B6N.FVB-Tg(Dmp1-cre)1Jqfe/BwdJ	The Jackson Laboratory	Strain #:023047 RRID:IMSR_JAX:023047
Mouse: B6.Cg-Igs2$^{tm1(CAG-mCherry,-cas9/ZNF10★)Mtm}$/J	The Jackson Laboratory	Strain #:030000 RRID:IMSR_JAX:030000
Mouse: B6.Cg-Gt(ROSA)26Sor$^{tm9(CAG-tdTomato)Hze}$/J	The Jackson Laboratory	Strain #:007909 RRID:IMSR_JAX:007909
Mouse: Tnfsf11-null	Xiong et al.[50]	N/A
Mouse: sgRNA^{Tnfsf11}	This paper	N/A
Mouse: Dmp1-dCas9::KRAB	This paper	N/A
Oligonucleotides		
Genotyping sgRNA^{Tnfsf11} mice: F2: 5′-AAGCACTTGCTCTCCCAAAG-3′ R2: 5′-GGCGGATCACAAGCAATAAT-3′ F3: 5′-GAGGGCCTATTTCCCATGAT-3′ R3: 5′-GGTGTTTCGTCCTTTCCACA-3′	This paper	N/A
Genotyping Dmp1-dCas9::KRAB mice: F1: 5′-CTTCGCTCTTTCACCCACAT-3′ R1: 5′- TACTGGGAGAGCACAGGACA-3′ R2″ 5′-GGCTCCGATCAGGTTCTTCT-3′	This paper	N/A
Genotyping Tnfsf11-null mice: RANKL-null-geno-for-1: 5′-CAGCTATGATGGAAGGCTCCTG-3′ RANKL-null-geno-rev-1: 5′-GATTGGCAAGGTAGGGTTCA-3′ RANKL-null-geno-for-2: 5′-TCTCAGGAGCTCCAGGTAAC-3′ RANKL-null-geno-rev-2: 5′-CGCTGGGCCACATCCAACTAA-3′	This paper	N/A
Taqman Gene Expression Assay Mrsp2	Life Technologies	Mm00475529_m1
Taqman Gene Expression Assay Actb	Life Technologies	Cat. #4352341E

(*Continued on next page*)

Continued

REAGENT or RESOURCE	SOURCE	IDENTIFIER
Taqman Gene Expression Assay Tnfsf11	Life Technologies	Mm00441906_m1
Taqman Gene Expression Assay Acp5	Life Technologies	Mm00475698_m1
Taqman Gene Expression Assay CtsK	Life Technologies	Mm00484039_m1

RESOURCE AVAILABILITY

Lead contact

Further information and requests for resources and reagents should be directed to and will be fulfilled by the lead contact, Melda Onal (monal@uams.edu).

Materials availability

Murine models generated in this study, namely sgRNA^{Tnfsf11} and Dmp1-dCas9::KRAB mice, will be made available upon request.

Data and code availability

- scRNA-seq data reported in this work are available at SRA database under accession number BioProject PRJNA896097. This paper does not report original code.
- Any additional information required to reanalyze the data reported in this paper can be obtained from the lead contact upon request.

EXPERIMENTAL MODEL AND SUBJECT DETAILS

Generation of mice

In previous studies, we have tested 3 sgRNAs targeting 3 different regions within 150 bp of the *Tnfsf11* transcriptional start site and determined the sgRNA that would facilitate efficient suppression of *Tnfsf11* via CRISPRi.[33] This sgRNA sequence was used to produce to sgRNA^{Tnfsf11} mice. These mice were produced via CRISPR/Cas9-mediated knock-in of a U6-sgRNA^{Tnfsf11} cassette into the Rosa26 locus. Briefly, Cas9 protein, a sgRNA targeting the Rosa26 locus (sgRNA^{Rosa26}), and single-strand oligonucleotide donor (ssODN) harboring the U6-sgRNA^{Tnfsf11} expression cassette, were used to perform the CRISPR/Cas9-mediated knock-in. sgRNA^{Rosa26} (ACTCCAGTCTTTCTAGAAGA, PAM: TGG) was used to drive the production of a double-strand break at the 1st intron of the *Rosa* loci.[51] A 756 bp ssODN was used to knock in the U6-sgRNA^{Tnfsf11} sequence into the sgRNA^{Rosa26} cleavage site. This ssODN contained the U6 small RNA promoter, sgRNA^{Tnfsf11} (GAGCCAATCAGCCTCCAGGA, PAM: GGG),[33] and homology arms corresponding to 200 bp upstream and downstream around the sgRNA^{Rosa} cleavage site. As the upstream homology arm of the ssODN contained the sequence targeted by sgRNA^{Rosa26}, the ssODN can be a target for CRISPR/Cas9 and sgRNA^{Rosa}. To avoid this, three nucleotides were changed in the upstream homology arm of the ssODN corresponding to the positions C9A, C13T, and G16A of the sgRNA^{Rosa} target sequence. Knock-in mice were produced by microinjection of 50 ng/ul Cas9 protein, 30 ng/ul sgRNA^{Rosa}, and 10 ng/ul ssODN into the pronuclei of C57BL/6J mice. Founders were screened for the presence of the knock-in sequence using the following primers: F1 5′-AAGCACTTGCTCTCCCAAAG-3′; R1 5′-GGCGGATCACAAGCAATAAT -3′. This PCR produced an 803bp band for the knock-in allele and a 447bp band for the wild-type allele. The structure of the knock-in allele was confirmed by DNA sequencing of the PCR product. The progeny of the founders were genotyped using the PCR primers indicated in key resources table. This PCR produced a 447 bp band for wild type allele and a 210bp band for the knock-in allele.

Dmp1-dCas9::KRAB mice were produced by Cyagen. For this purpose, a cassette containing nuclear localization signal-dCas9-KRAB-rabbit beta globin poly-A terminator (NLS-dCas9-KRAB-rBG pA) sequences was inserted upstream of ATG start codon in exon 2 of the endogenous murine *Dmp1* gene. The *Dmp1* targeting vector used for the knock-in contained homology arms, NLS-dCas9-KRAB-rBG pA cassette, and a Neo cassette flanked by self-deletion anchor sites. This targeting construct was linearized by restriction digestion and electroporated into C57BL/6N ES cells. The electroporated ES cells were subjected to G418 selection followed by expansion of G418-resistant clones. Insertion of the targeting cassette was confirmed by PCR and Southern blot analysis. After the removal of the Neo cassette, ES cells with the correct insertion were introduced into host embryos and transferred into surrogate mothers. Chimeras were

bred to wild-type mice to confirm germline transmission. Pups were genotyped by PCR to identify F1 heterozygous mutants. Genotyping was performed with the PCR primers indicated in key resources table. This PCR produced a 202 bp band for wild type allele and a 343bp band for the knock-in allele.

A Tnfsf11-null allele was created as a by-product of generating the Tnfsf11-SR allele using gene editing.[50] The null allele contains a single T insertion after the 18th nucleotide of exon 4, which results in truncation of the RANKL protein prior to production of the TNF domain. Genotyping was performed with the PCR primers indicated in key resources table. All 4 primers were used in a single PCR to detect the single T insertion via the following product sizes: WT product = 231 bp, null product = 135 bp.

Murine models

Generation and genotyping of the *Tnfsf11*^{floxed} [23], Dmp1-Cre[6] and H11^{dCas9KRAB}[38,39] mice used in this study have been described previously. Briefly, *Tnfsf11*^{floxed} mice were created by flanking exon 3 and exon 4 of *Tnfsf11* with loxP sites. In Dmp1-Cre transgenic mice, a 14 kb Dmp1 promoter fragment, which contains the genomic sequence of the promoter through 17 bp of the initial non-coding region in exon 2, drives the Cre expression. H11^{dCas9KRAB} knock-in mice constitutively active and broadly expressed CMV early enhancer/chicken β actin (CAG) promoter drives the expression of mCherry and dCas9::KRAB from the safe harbor *Igs2* locus (Hipp11 or H11). All mice were provided water and food *ad libitum* and were maintained on a 12-hour light/dark cycle. All animal studies were carried out in accordance with the policies of, and with approval from, the Institutional Animal Care and Use Committee of the University of Arkansas for Medical Sciences. The studies of this manuscript were performed and reported in accordance with ARRIVE guidelines. Sex, number and age of the experimental mice are indicated in each figure legend.

METHOD DETAILS

RNA isolation and gene expression analysis

Murine bones and soft tissues were snap-frozen in liquid nitrogen and stored at −80°C. To prepare RNA, frozen thymus, spleen, lumbar vertebrae, tibia shafts, and calvaria were homogenized in Trizol Reagent (Life Technologies # 15596018). RNA was isolated from soft tissues following the Trizol Reagent's manufacturer protocol. RNA was isolated from bones using RNAeasy Plus Mini Kit (Qiagen Cat # 74136) according to the manufacturer's instructions. For all tissues, RNA concentrations were determined using a Nanodrop instrument (Thermo Fisher Scientific). One μg of RNA was used to synthesize cDNA using a High-Capacity cDNA Reverse Transcription Kit (Applied Biosystems Cat. #4368814) according to the manufacturer's instructions. Relative mRNA levels were determined using multiplex quantitative real-time PCR (qRT-PCR) analysis using TaqMan Fast Advanced Master Mix (Applied Biosystems # 4444964), FAM-labeled TaqMan gene expression assays (Life Technologies) and VIC-labeled mouse *Mrsp2* (Mm00475529_m1) or VIC-labeled mouse *Actb* (beta-actin)(Applied Biosystems Cat. #4352341E). The relative mRNA levels were determined using the comparative cycle threshold (ΔCt) method.[52]

Skeletal analysis

Bone mineral density (BMD) was measured in live mice by dual-energy x-ray absorptiometry with a PIXImus Mouse Densitometer (GE Lunar Corp., Madison, WI) using the manufacturer's software as described previously (PMID: 25431114). X-ray images of euthanized mice were taken using a Faxitron imager. Fourth lumbar vertebrae (L4) and femurs were used for the microCT analysis. The femurs and vertebrae were dissected, cleaned of soft tissue, wrapped in saline-soaked gauze, and stored at –20°C. For microCT analysis, bones were thawed and loaded into a 12.3 mm diameter scanning tube filled with saline. The microCT scans were performed on a model uCT40 (Scanco Biomedical) as previously described.[53,54] Briefly, medium-resolution scans were obtained (12 μm isotropic voxel size). A Gaussian filter (sigma = 0.8, support = 1) was used to reduce noise, and a threshold of 220 was used for all scans. Nomenclature conforms to recommendations of the American Society for Bone and Mineral Research.[55] The femurs were scanned from the distal growth plate to the mid-shaft. The midshaft cortical measurements were performed by drawing contours to measure the cortical thickness on the first 20 midshaft slices. For microCT analysis of the fourth lumbar vertebrae (L4), the whole vertebral body was scanned. Trabecular analysis was performed by drawing contours every 10 slices on the whole space between the 2 growth plates of the vertebrae. Similar to femoral measurements, the vertebral cortical bone thickness was determined on the ventral cortical wall using contours of cross-sectional images, drawn to exclude trabecular bone. Calibration and quality control of the scanner were performed weekly or monthly as previously described.[33]

scRNA-seq sample preparation

Muscles and soft tissue were removed from freshly isolated femurs and tibias. The periosteum was removed by scraping with a scalpel. Epiphyses were removed above the growth plate. Bones (containing cancellous and cortical compartments) were cut longitudinally and flushed with PBS containing 1% BSA to remove marrow. Bone was then chopped into small fragments and subjected to 5 serial digestions with LiberaseTM (Roche, Sigma Cat. #LIBTM-RO) interspaced with incubation in EDTA. Briefly, for each enzyme digestion, bone fragments were incubated in HBSS containing 2 Wunsch units of LiberaseTM for 20 minutes (min) at 37°C with shaking. The supernatant of each fraction was moved to a new tube on ice. After each enzyme digestion bone fragments were washed with PBS. Bone fragments were then incubated with PBS containing 5 mM EDTA and 0.1% BSA for 20 min at 37°C with shaking. The supernatant of each fraction was transferred to a fresh tube on ice. After each EDTA treatment, bone fragments were washed with HBSS. Cells isolated from each fraction were pelleted at 300 g for 10 min and supernatants were aspirated with a glass pipette. Pelleted cells were resuspended in the FACS sorting buffer (PBS with 1% BSA with 2 mM EDTA) and stored on ice. Fractions 2 to 8 were combined, concentrated, and used for FACS. Approximately 10, 000 TdTomato-positive cells were sorted into a fresh tube. Single cells were captured as droplets using a 10x Genomics Chromium Controller. scRNA-seq libraries were constructed using Chromium Single-Cell 3′ v3 Reagent Kit according to the manufacturer's instructions.

scRNA-seq data analysis

The raw sequencing data (fastq files) were preprocessed by CellRanger software (10x Genomics) version 6.0.1. Reads were aligned on *Mus musculus* reference genome (mm10) and demultiplexed to generate count tables of transcripts across individual cells. The count tables were further analyzed in R suite software through Seurat version 4.1.0 package.[56] Cells with a gene number less than 500, greater 3,500, and having more than 10% of unique molecular identifiers stemming from mitochondrial genes, were discarded from the analysis. Principal component analysis (PCA) was performed on the top 6,000 variable genes of the remaining high-quality cells. To make the data across individual samples comparable, we performed integration across samples using the reciprocal PCA method to minimize the technical batch effect. To identify cell types, clustering analysis of Louvain algorithm with multilevel refinement[57] was employed. The clustering result was visualized by Uniform Manifold Approximation and Projection for Dimension Reduction (UMAP) method of two dimensions. The gene-specific markers of individual clusters were identified by the MAST method.[58]

QUANTIFICATION AND STATISTICAL ANALYSIS

All values are reported as mean ± standard deviation (STDEV). The statistical tests performed are indicated in figure legends. Briefly, using SAS version 9.4, one-way ANOVA models were fit to the various outcomes with animal group as the predictor variable. Model residuals were examined for normality and constant variance. Transformations such as square root, natural logarithm, negative reciprocal or rank were used when the original scale of data did not meet those assumptions. In case of normality, statistical comparisons of two groups were done by t-test (equal variance) or by t-test with Welch correction (unequal variance). In case where data does not have a normal distribution, statistical comparisons of two groups were done by rank sum test. All pairwise comparisons from each ANOVA were examined and the Tukey method was used to adjust the p values for multiple comparisons.

SAS v9.4 software was used for the comparison of the phenotype effect between the two ages in Figure 4. First, vertebral, femoral, and global BMD were analyzed from the 4 genotypes and 2 ages. Two-way ANOVAs with the factors of genotype and age were performed to check for differences between the 3 control groups at each age. No significant differences were found while the assumptions of normally distributed residuals with equal variance were verified for all 3 BMD sites. Next, having verified no statistically significant differences between the control groups, the control groups were combined with new Two-way ANOVAs with the factors of age (12 months vs. 4 months) and experimental group (experimental vs. control). Again the assumptions of normally distributed residuals with equal variance were verified for all three BMD sites. A contrast was estimated for each model testing for an interaction effect of the experimental group and age, to address if the change between 12 months and 4 months for the experimental group was equal to or different from that change within the control group. *t*-tests on this contrast were performed for all 3 BMD sites.